JACS
JOURNAL OF THE AMERICAN CHEMICAL SOCIETY
Article
pubs.acs.org/JACS

Real-Time Discrimination and Versatile Profiling of Spontaneous Reactive Oxygen Species in Living Organisms with a Single Fluorescent Probe

Ruilong Zhang,[†,‡,#] Jun Zhao,[†,#] Guangmei Han,[†,#] Zhengjie Liu,[†,‡] Cui Liu,[†,‡] Cheng Zhang,[†,‡] Bianhua Liu,[†] Changlong Jiang,[†] Renyong Liu,[†] Tingting Zhao,[†] Ming-Yong Han,[†,§] and Zhongping Zhang*[,†,‡,∥]

[†]CAS Center for Excellence in Nanoscience, Institute of Intelligent Machines, Chinese Academy of Sciences, Hefei, Anhui 230031, China

[‡]Department of Chemistry, University of Science and Technology of China, Hefei, Anhui 230026, China

[§]Institute of Materials Research and Engineering, A-STAR, 3 Research Link, Singapore 117602

[∥]State Key Laboratory of Transducer Technology, Chinese Academy of Sciences, Hefei, Anhui 230031, China

Supporting Information

ABSTRACT: Fluorescent probes are powerful tools for the investigations of reactive oxygen species (ROS) in living organisms by visualization and imaging. However, the multiparallel assays of several ROS with multiple probes are often limited by the available number of spectrally nonoverlapping chromophores together with large invasive effects and discrepant biological locations. Meanwhile, the spontaneous ROS profilings in various living organs/tissues are also limited by the penetration capability of probes across different biological barriers and the stability in reactive in vivo environments. Here, we report a single fluorescent probe to achieve the effective discrimination and profiling of hydroxyl radicals (•OH) and hypochlorous acid (HClO) in living organisms. The probe is constructed by chemically grafting an additional five-membered heterocyclic ring and a lateral triethylene glycol chain to a fluorescein mother, which does not only turn off the fluorescence of fluorescein, but also create the dual reactive sites to ROS and the penetration capability in passing through various biological barriers. The reactions of probe with •OH and HClO simultaneously result in cyan and green emissions, respectively, providing the real-time discrimination and quantitative analysis of the two ROS in cellular mitochondria. Surprisingly, the accumulation of probes in the intestine and liver of a normal-state zebrafish and the transfer pathway from intestine-to-blood-to-organ/tissue-to-kidney-to-excretion clearly present the profiling of spontaneous •OH and HClO in these metabolic organs. In particular, the stress generation of •OH at the fresh wound of zebrafish is successfully visualized for the first time, in spite of its extremely short lifetime.

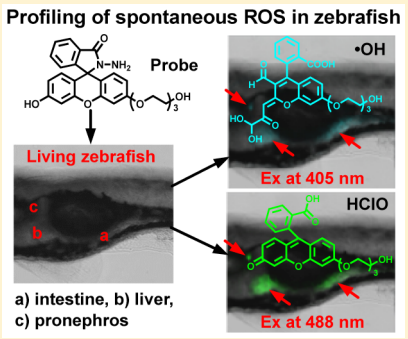

INTRODUCTION

Reactive oxygen species (ROS) are mostly produced in the cellular mitochondria of various organs and tissues of living organisms via the incomplete reduction of molecular oxygen, which is greatly intensified under external stimulations and injuries.[1−5] On the one hand, the highly active ROS play a key role in cell signaling, homeostasis, energy production and defense mechanism against infection to regulate a wide range of biological or pathological functions,[2−5] but on the other hand the excessive generation of ROS may also cause cell aging, DNA/protein mutations and various diseases.[6] As evidenced in the recent studies,[6,7] every individual ROS can have complex/diverse functions, which still remains ambiguous in many aspects. In practical cases, multiple ROS including hydroxyl radicals (•OH), hypochlorous acid (HClO), hydrogen peroxide (H_2O_2), superoxide radicals ($O_2•^-$) and singlet oxygen ($^1O_2$) commonly coexist in vivo, and further increase the difficulty in understanding their individual functions. Among ROS, the transformations also widely occur in living systems (e.g., from $O_2•^-$ to H_2O_2 and from H_2O_2 to HClO).[5] Accordingly, there is a great demand to develop a novel approach to the real-time discriminations and quantitative assays of ROS in living systems, providing a powerful tool to reveal their functions and correlations.

The most classical analysis of ROS is carried out via electron spin resonance measurement by using a radical trapping agent, but it requires an expensive spectrometer and is still difficult to be employed in cells and in vivo. Recently, considerable efforts have been devoted to the development of chemosensors for the detection of ROS using the molecular or nanoscaled probes through the specific reactions with ROS and the signal readouts

Received: December 9, 2015
Published: March 3, 2016

DOI: 10.1021/jacs.5b12848
J. Am. Chem. Soc. 2016, 138, 3769−3778

Scheme 1. (A) Synthetic Route of Probe FHZ; (B) Reaction Mechanisms of FHZ with •OH and HClO

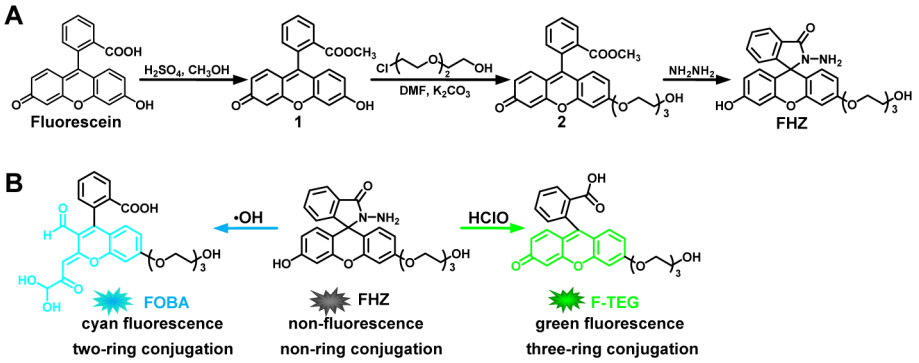

including fluorescence,[8−14] Raman,[15] chemiluminescence[16] and etc. Among them, fluorescent probes are most widely used to monitor ROS in living systems due to the advantages in sensitivity, real-time imaging and visualization. A general strategy is to conjugate an organic dye or luminescent nanoparticle with a recognition element for specifically trapping and reacting with a target ROS, such as •OH-induced cleavage of DNA strand,[17,18] HClO oxidation of *p*-methoxyphenol,[19,20] and $^1O_2$-induced formation of endoperoxide,[21,22] in which the fluorescent "turn on" or "turn off" responses indicate the presence and level of ROS. On the basis of the one-to-one principle, the parallel assays of several ROS can be performed with the use of multiple fluorescent probes specific to different ROS.[23] However, the scenario of multiple probes is greatly limited by spectrally nonoverlapping chromophores, and large invasive effects, and discrepant biological distributions of probes.[11,24] Moreover, the difference in lifetimes of ROS further increases the difficulty to design multiple probes. Up to date, the approach of a single fluorescent probe to the simultaneous detections of several ROS has still been a challenging task.

Thus, it is ideal to develop a single fluorescent probe with different reactive sites that can respond to several ROS with the distinguishable fluorescent signals. However, most of reported fluorescent probes contain only one reactive site with ROS by the specific or nonspecific reactions, leading to the same fluorescence readout to individual or multiple ROS. Furthermore, the penetration capability in passing through various biological barriers also limits the applicable range of many fluorescent probes for imaging the ROS in various organs/tissues. In this current work, we have synthesized a dual reactive-site probe by the reconstruction of fluorescein molecule to obtain the dual reactivities specific to •OH and HClO, and the high biocompatibility in the reactive in vivo environments. The simultaneous reactions of probe with •OH and HClO generate two different products with cyan and green emissions, respectively, which can effectively achieve the real-time discrimination of the two ROS. On the basis of these investigations, the unique applications in the profiling of spontaneous ROS in living organs and tissues have successfully been demonstrated.

RESULTS AND DISCUSSION

Synthesis of Fluorescent Probe. A common fluorescent dye, fluorescein, was chosen as the starting molecule to synthesize the fluorescent probe, 6-triethylene glycol substituted fluorescein hydrazide (FHZ), through three-step reactions as illustrated in Scheme 1A. First, the carboxyl group of fluorescein was protected by reacting with methanol to form a methyl ester group in the presence of concentrated sulfuric acid. Second, the aromatic ring of fluorescein was grafted with a triethylene glycol by substituting a hydrogen atom with 2-[2-(2-chloroethoxy)-ethoxy]ethanol, and the formed lateral chain greatly enhanced the hydrophilicity and biocompatibility of probe. Third, the methyl ester group reacted with hydrazine hydrate via hydrazinolysis to produce the final product FHZ, leading to the nonconjugation among three aromatic rings due to the formation of a new five-membered heterocyclic ring. The resulting FHZ completely switched off the strong fluorescence originating from the three conjugated aromatic rings of fluorescein. After purification, the structure of FHZ was confirmed by ^{1}H NMR, ^{13}C NMR and HR-MS (Figures S1−S3).

Reactions of FHZ with •OH and HClO. Fluorescein emits strong green fluorescence at 520 nm excited at its absorption maximum of 490 nm, while its fluorescein-hydrazine derivative FHZ becomes nonfluorescent because the newly formed five-membered ring breaks the conjugated system of fluorescein chromophore and induces the decrease of electron delocalization (Scheme 1B, Figure S4). Scheme S1 illustrates the reaction mechanisms of FHZ with •OH and HClO. In the presence of •OH, one of hydrogen atoms in the aromatic rings of FHZ is first substituted by •OH to form an intermediate product FHZ−OH (see the ^{1}H NMR and MS spectra in Figures S5 and S6, respectively). With ultrastrong oxidizability, •OH radicals then simultaneously break the bottom-left aromatic ring and the five-membered ring of FHZ to form the final product FOBA with two conjugated aromatic rings, giving off strong cyan fluorescence (Scheme S1A).[25,26] The fluorescence undergoes a hypsochromic shift from green to cyan due to the decreased size of conjugated system (Figure S4B). FOBA was characterized by ^{1}H NMR and MS spectra (Figures S7 and S8).

Interestingly, the isomer of FHZ with a C═N bond[27] can also proceed an addition reaction with HClO to form a highly unstable intermediate product (Scheme S1B). After the loss of a water molecule, the intermediate product FHZ-Cl is monitored by MS spectroscopy (Figure S9). The lateral group of N-chloro amide is finally cleaved from the mother molecule, and then the final product F-TEG is formed and characterized by ^{1}H NMR and MS spectra (Figures S10 and S11). With the same conjugated structure as fluorescein, F-TEG remains to emit strong green fluorescence at 520 nm.

Fluorescent "Turn-On" Responses to •OH and HClO. The reaction mechanisms have further been demonstrated by the fluorescent responses of FHZ to •OH and HClO in PBS buffer (pH 7.2). Here, •OH was supplied via Fenton reaction

DOI: 10.1021/jacs.5b12848
J. Am. Chem. Soc. 2016, 138, 3769−3778

between $FeSO_4$ and H_2O_2. When H_2O_2 was titrated into the mixture of 10 μM FHZ and 1 mM $FeSO_4$ in PBS buffer, the resultant •OH reacted immediately with FHZ and the fluorescent spectra were recorded with the addition of H_2O_2 (Figure 1A). A fluorescent peak at 486 nm began to appear at

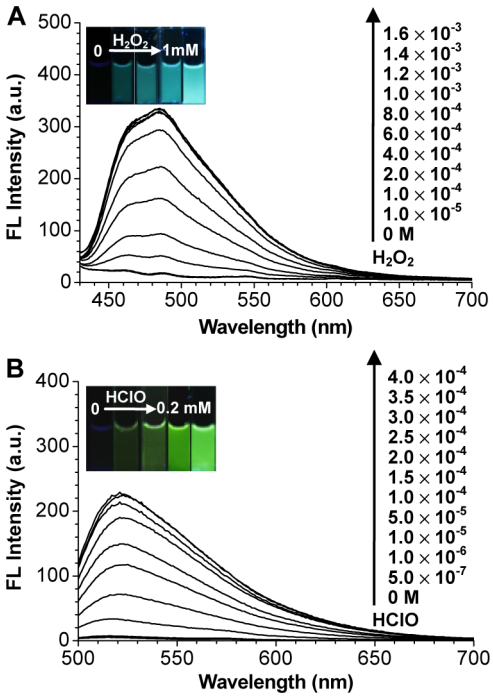

Figure 1. (A) Fluorescent spectra of 10 μM FHZ with the addition of H_2O_2 in the presence of 1 mM $FeSO_4$ at the excitation wavelength of 410 nm. The •OH radicals were supplied via Fenton reaction between $FeSO_4$ and H_2O_2. (B) Fluorescent spectra of 10 μM FHZ with the addition of HClO at the excitation wavelength of 490 nm. The insets are the corresponding photographs under 365 nm UV lamp.

10 μM H_2O_2 with the excitation at 410 nm and increasingly intensified with the concentration up to 1 mM. The enhancement of fluorescence intensity reached the maximum of ~19.1 folds that of blank FHZ at 1 mM H_2O_2. The fluorescence intensities showed a good linearity against the H_2O_2 concentrations in the range from 10 μM to 1 mM with standard deviation R^2 = 0.9945 (Figure S14), suggesting that FHZ can be used for the quantification of •OH. At the same time, the solution changed from colorless to bright cyan under UV lamp (the inset in Figure 1A).

The same experiments were performed by the addition of HClO into 10 μM FHZ in PBS buffer (Figure 1B). Different from the addition of •OH, the fluorescent peak appeared at 520 nm and the optimal excitation wavelength was 490 nm (Figures S15 and S16), which were similar to those of fluorescein due to the identical chromophore of F-TEG to fluorescein. The fluorescence intensity very slowly enhanced in the range of 0.5−10 μM HClO, and then remarkably enhanced upon the HClO concentration over 10 μM. The maximal enhancement reached ~34.3 times at 300 μM HClO. Even if HClO concentration was as low as 0.5 μM, the fluorescence was still enhanced by ~20%, suggesting an ultrasensitive response of FHZ to HClO. The dose-dependent fluorescence intensities also exhibited a good linearity against the HClO concentrations in the range of 20 to 200 μM with standard deviation R^2 = 0.9960 (Figure S17). Meanwhile, the green fluorescence could be clearly seen under UV lamp (the inset in Figure 1B).

Dual Fluorescent Responses to the Coexisting •OH and HClO. The coexistence of •OH and HClO is very common in living systems, and we thus examined the fluorescent responses of FHZ to the coexisting •OH and HClO species. After 50 μM FHZ and 1 mM $FeSO_4$ were mixed in PBS buffer, 1 mM H_2O_2 and 500 μM HClO were synchronously/slowly injected into the mixture through two syringes under vigorously stirring. The fluorescent spectra were collected using the excitation wavelengths of 410 and 490 nm. The two fluorescent peaks at 486 and 520 nm were detected (Figure S18), and corresponded to those in the separate reaction systems as shown in Figure 1. That is to say, probe FHZ can give out two different fluorescent signals in the presence of both •OH and HClO, suggesting the synchronous discrimination of •OH and HClO by a dual-channel detection model with two exciting wavelengths.

In the synchronous determinations, the spectral overlap of fluorescent responses to •OH and HClO can be overcome by the two exciting wavelengths and two collection windows (430−490 nm; 510−560 nm). Table S1 shows the fluorescence quantum yields of FHZ, FOBA and F-TEG (0.01, 0.42 and 0.34, respectively) and the molar extinction coefficients and the fluorescent brightnesses at the given wavelengths for each molecule. In theory, the brightness is calculated by the equation (extinction coefficient × quantum yield)/1000. From Table S1, FHZ is nonfluorescent under the excitation of both 410 and 490 nm, and meanwhile the products FOBA and F-TEG exhibit very large differences in fluorescent brightnesses with the excitation wavelengths of 410 and 490 nm. These indicate that the collected fluorescences from the two excitations can greatly reduce the interference from spectral overlap. Moreover, the ranges of collection windows further suppress the negative effects of spectral overlap to a small error range (<5%) on confocal microscopy. Figure S19 gives the spectral simulation and analysis on the interference with the above experimental conditions.

Dynamics and Selectivity. In general, most of ROS are of short lifetimes in living systems and thus require a desirable probe with fast reaction dynamics to them. Figure 2A shows the time-dependent fluorescence intensities of FHZ to •OH and HClO at the constant concentrations. Upon the addition of •OH (200 μM H_2O_2 and 1 mM $FeSO_4$), the fluorescence immediately increased and reached the maximum value in ~1 min. The similar fluorescence enhancement was also observed in the case of HClO, and the fluorescence intensity reached the maximum value in ~2 min. With prolonging the reaction time, the fluorescence intensities almost kept unchanged in the two systems, indicating that the reactions of FHZ with •OH and HClO were completed in 1 and 2 min, respectively. The very fast dynamics are significantly beneficial to track the in situ generations of ROS in living systems.

The selectivity of FHZ to •OH and HClO was also examined by the addition of other typical ROS and reactive nitrogen species (RNS) such as H_2O_2, $^1O_2$, $O_2•^-$, NO, $ONOO^-$ into FHZ solution (Figure 2B). Among them, HClO, H_2O_2, $^1O_2$, $O_2•^-$, NO and $ONOO^-$ did not cause any significant enhancement of cyan fluorescence with the excitation at 410 nm, but •OH (1 mM H_2O_2 and 1 mM $FeSO_4$) resulted in ~19 folds fluorescence enhancement. On the other hand, •OH, H_2O_2, $^1O_2$, $O_2•^-$, NO and $ONOO^-$ could not cause any enhancement of green fluorescence with

DOI: 10.1021/jacs.5b12848
J. Am. Chem. Soc. 2016, 138, 3769−3778

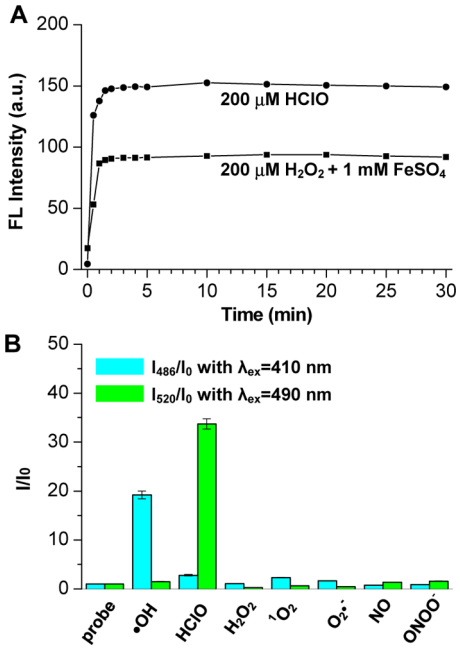

Figure 2. (A) Time-dependent fluorescence intensities of FHZ (10 μM) in the presence of •OH (200 μM H_2O_2 and 1 mM $FeSO_4$) and HClO (200 μM) for 30 min at room temperature. (B) The selectivity of fluorescent responses (I/I_0) to various ROS/RNS in 10 μM FHZ PBS buffer (•OH: 1 mM $FeSO_4$ and 1 mM H_2O_2; HClO: 1 mM NaClO; H_2O_2: 1 mM H_2O_2; $^1O_2$: 1 mM H_2O_2 and 1 mM NaClO; $O_2•^-$: 1 mM KO_2; NO: 1 mM NONOate; $ONOO^-$: 1 mM $NaNO_2$ and 1 mM H_2O_2). The error bars represent the mean errors from the results of 5 tests.

the excitation at 490 nm, while 1 mM HClO led to ~35 folds fluorescence enhancement. Therefore, probe FHZ shows very high specificity to the detections of •OH and HClO with the excitations at 410 and 490 nm, respectively.

Visualizations of •OH and HClO in Cells. Before the bioimaging employments, our experiments had evidenced the almost nonbiotoxicity of probe FHZ to cells (Figure S20). Due to the spectral overlap of FOBA and F-TEG (Figure 1), we used a dual-channel mode in the detections of •OH and HClO in living cells. Cyan channel for the detection of •OH was set with the excitation at 405 nm and the emission collection at 430−490 nm. Meanwhile, green channel for the detection of HClO was excited at 488 nm and the emission was collected at 510−560 nm. It should be noted that the used excitation wavelengths (405 and 488 nm) have very small deviations from the optimal excitations at 410 and 490 nm, because the wavelengths of laser source of confocal microscope are fixed at 405 and 488 nm.

Figure 3 shows the individual and simultaneous determinations of •OH and HClO spiked in HeLa cells. In the column A, the cells were incubated with probe FHZ and then treated with H_2O_2 and EDTA-Fe^{2+}. The bright fluorescence from cyan channel was definitely observed and the fluorescence intensity gradually increased with the concentration of •OH (Figure S21). However, only very weak fluorescent signal was detected from the green channel (Figure 3A). In the case of HClO, contrarily, the cells displayed bright fluorescence from the green channel (Figure 3B), following the remarkable enhancement dependent on the dose of HClO (Figure S21). Meanwhile, only weak fluorescence was detected from the cyan channel. Furthermore, we examined the ability of the probe FHZ for the simultaneous determinations of •OH and

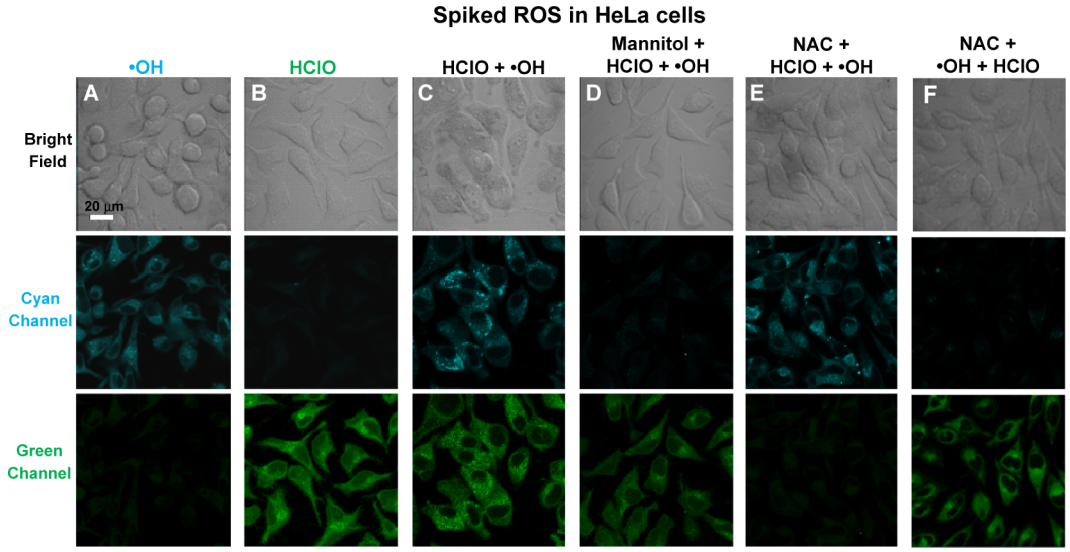

Figure 3. Individual and simultaneous determinations of •OH and HClO spiked in HeLa cells. The cyan and green channels were excited with 405 and 488 nm, and collected at the windows of 430−490 and 510−560 nm, respectively. Before the fluorescent imaging, each treatment/incubation of cells with different reagents kept 30 min, and then the cells were washed with PBS buffer three times. (A) The visualization of •OH (HeLa cells were incubated with 50 μM FHZ, and then treated with 1 mM H_2O_2 and 1 mM EDTA-Fe^{2+} to supply •OH). (B) The visualization of HClO (HeLa cells were incubated with 50 μM FHZ, and then treated with 200 μM HClO). (C) The simultaneous visualizations of •OH and HClO (HeLa cells were incubated with 100 μM FHZ, and then treated with 200 μM HClO, 1 mM H_2O_2 and 1 mM EDTA-Fe^{2+} in order). (D) The control experiments by adding •OH scavenger, mannitol (HeLa cells were treated with 2 mL of 100 mM mannitol for 30 min and then washed with PBS buffer, and finally incubated with 2 mL of 100 μM FHZ, 200 μM HClO, 1 mM H_2O_2 and 1 mM EDTA-Fe^{2+} in order). (E) The control experiments by adding *N*-acetyl-L-cysteine (NAC), a scavenger of both HClO and •OH (HeLa cells were treated with 2 mL of 10 mM NAC and then washed with PBS buffer, and finally incubated with 2 mL of 100 μM FHZ, 200 μM HClO, 1 mM H_2O_2 and 1 mM EDTA-Fe^{2+} in order). (F) The control experiments by changing the sequence of cell treatments as NAC, FHZ, EDTA-Fe^{2+}, H_2O_2 and HClO in order.

DOI: 10.1021/jacs.5b12848
J. Am. Chem. Soc. 2016, 138, 3769−3778

HClO in living cells (Figure 3C). After loaded with probe FHZ and treated with HClO and H_2O_2/EDTA-Fe^{2+} in order, HeLa cells displayed the bright fluorescences from both cyan and green channels, similar to the two separate detections in Figure 3A and B. The performances of FHZ demonstrate its capability of simultaneously monitoring the intracellular •OH and HClO species.

The control experiments in Figure 3D−F confirm that the fluorescence enhancements observed above were indeed induced by •OH and HClO. HeLa cells were incubated with the •OH scavenger mannitol and then treated with FHZ, HClO, H_2O_2 and EDTA-Fe^{2+} in order. The cells only gave out strong fluorescence from green channel, while the cyan fluorescence resulting from •OH was not almost observed (Figure 3D), indicating that the bright cyan fluorescences in Figure 3A and C resulted from the sufficient generation of •OH by the Fenton reaction in cells. Moreover, *N*-acetyl-L-cysteine (NAC), a scavenger of both HClO and •OH,[28] was also used in other two control experiments. HeLa cells were treated with NAC, FHZ, HClO, and H_2O_2/EDTA-Fe^{2+} sequentially (Figure 3E). After the addition of HClO, NAC was mostly consumed by the reaction with HClO, and thus the green fluorescence resulting from HClO did not light up. With the further addition of •OH (H_2O_2/EDTA-Fe^{2+}), there was a very less amount of NAC existing in the cells, and thus the cyan fluorescence resulting from •OH could still be seen by the reaction with FHZ. These provide unambiguous evidence that the green fluorescence in Figure 3B and C resulted from the reaction of probe with HClO. It should be noted that higher concentration of NAC leads to the death of cells. Figure 3F shows another control experiment with the changed addition sequence as NAC, FHZ, EDTA-Fe^{2+}/H_2O_2 and HClO in order. Contrarily, the cyan fluorescence was greatly suppressed, but the green fluorescence only reduced in a small degree. The above results indicate that the fluorescent signals originate from the reactions of FHZ with HClO and •OH.

Determinations of Endogenous •OH and HClO. Mitochondria are the energy factory of cells by respiratory actions, which produces a large amount of ROS there. In the present work, we tried to visualize the endogenous •OH and HClO via the stimulation of drug in cellular mitochondria. After RAW 264.7 macrophages were loaded with probe FHZ, the cells were then treated with a typical apoptotic drug, phorbol 12-myristate 13-acetate (PMA) to generate ROS in mitochondria.[8,11,29] Obviously, the cells showed the bright fluorescences from both cyan and green channels (Figure 4B and C). Meanwhile, a commercially available mitochondrial dye (MitoTracker Red CMXRos) was employed for the colocalization study (Figure 4D). As shown in Figure 4E and F, the fluorescent images from cyan and green channels overlapped with the image of mitochondrial sites with colocalization coefficients of 0.76 and 0.82, respectively. On the other hand, the control experiments by adding the ROS scavengers in the PMA stimulation tests led to the decrease/disappearance of corresponding fluorescences (Figure S23). These observations indicate that the probe FHZ can efficiently enter the cellular mitochondria and exhibit the differentiable/visual capabilities to the endogenous •OH and HClO by the dual fluorescent responses.

In fact, probe FHZ is not specific for mitochondria, but rather distributes in cytoplasm and can also spread into mitochondria, which is confirmed by the exogenous addition of ROS in macrophages (Figure S24). When PMA stimulates the

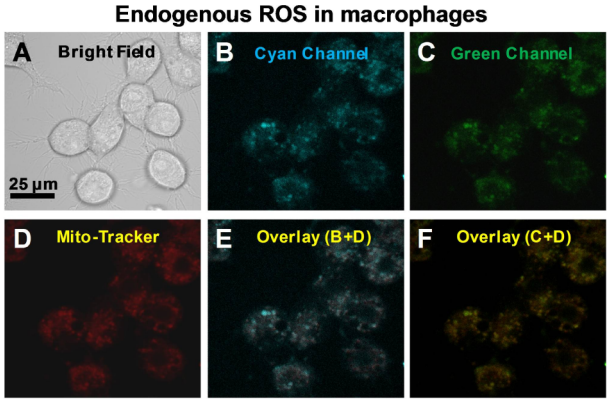

Figure 4. Simultaneous determinations of endogenous •OH and HClO in cellular mitochondria. RAW 264.7 macrophages were incubated with 100 μM FHZ for 30 min. After washed with PBS buffer, the cells were then treated with 2 μg/mL PMA for 4 h and 5 μM MitoTracker Red CMXRos for another 30 min. (A) Bright field image of the macrophages. (B) Fluorescent image from cyan channel. (C) Fluorescent image from green channel. (D) Fluorescent image from MitoTracker Red CMXRos channel (excited at 633 nm and collected at 650−700 nm). (E) Overlay of (B) and (D). (F) Overlay of (C) and (D).

mitochondria of macrophages to produce a large amount of ROS, the fluorescence of mitochondria is thus lighted up by the probe, but the fluorescence of cytoplasm is very weak due to the low level of ROS there.

Quantitative Correlations of Endogenous •OH and HClO. Further, we tested the capability of FHZ to quantify •OH and HClO in mitochondria to clarify their correlations. The experiments were performed by recording the time-/dose-dependent evolutions of fluorescence intensities in mitochondria with the stimulation of PMA. The fluorescence intensities were spectrally integrated from the cyan channel of 430−490 nm and the green channel of 510−560 nm.

After RAW 264.7 macrophages were loaded with probe FHZ and incubated with 2.0 μg/mL PMA, the temporal observations showed that fluorescences of mitochondria from cyan and green channels became gradually brighter in a time period of 0−4 h (Figure 5A). The mean intensities collected from the two channels increasingly enhanced in the observation time of 3 h, and finally tended to stability in 4 h (Figure 5B). The quantitative measurements suggest that the amounts of •OH and HClO in mitochondria rapidly increased to ∼3.6 and ∼2.6 folds in 3 h, respectively, by the stimulation of PMA. In parallel, RAW 264.7 macrophages were incubated with different doses of PMA for the same period of 4 h, and the dose-dependent fluorescent images were shown in Figure 5C. The fluorescences of mitochondria from both cyan and green channels became much stronger with the amount of PMA. The mean fluorescence intensities in Figure 5D revealed that the amounts of •OH and HClO in mitochondria were highly correlated with the dose of PMA. Even 1.0 μg/mL PMA can effectively induce the macrophages to release ∼2.8 folds •OH and ∼2.1 folds HClO. However, the enhancement effect became much weaker when the concentration of PMA was higher than 1.5 μg/mL. The temporal and dose-dependent experimental results further confirm the quantitative determinations of •OH and HClO in mitochondria by probe FHZ.

In living systems, •OH and HClO are closely correlated species originating from the H_2O_2. While •OH radicals are

DOI: 10.1021/jacs.5b12848
J. Am. Chem. Soc. 2016, 138, 3769−3778

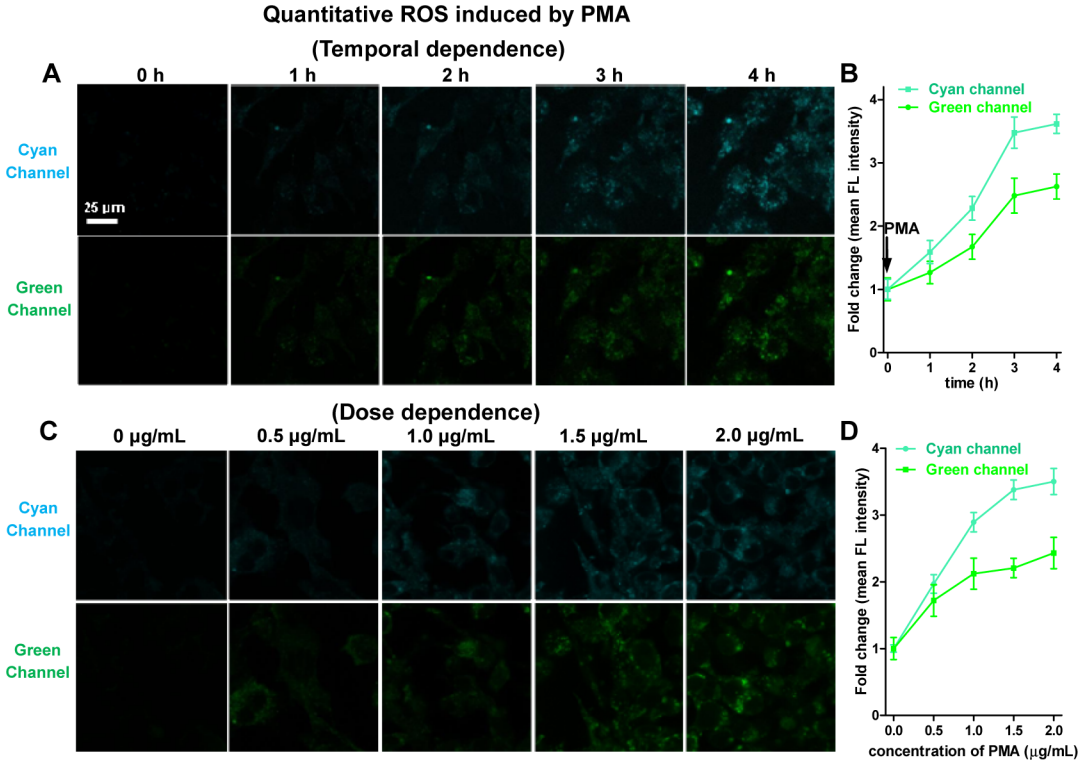

Figure 5. Quantitative determinations of •OH and HClO in mitochondria. RAW 264.7 macrophages were incubated with 100 μM FHZ, and then washed with PBS. (A) Time-dependent fluorescent images from the cyan and green channels after the cells were further treated with 2.0 μg/mL PMA. (B) Time-dependent evolutions of mean fluorescence intensities. Six cells with the almost similar sizes were manually selected to collect the time-dependent fluorescence intensities, and the mean fluorescence intensities at each time point were calculated from the six intensities. The fold of fluorescence intensity is compared to that at the zero time point. The error bars represent standard deviation (±SD). (C) Dose-dependent fluorescent images from the cyan and green channels after the cells were further treated with different amounts of PMA for 4 h. (D) Dose-dependent evolutions of mean fluorescence intensities. Six fields (0.05 × 0.05 mm^2) were selected at each dose, in which each field contained one similar-sized cell. The fluorescence intensities were collected from the six images with the identical observation area. The error bars represent standard deviation (±SD). All these above quantification experiments were repeated with three batches of cells.

produced via Fenton or Habber−Weiss reactions, HClO is also formed by the peroxidation of chloride ions (Cl^-) with H_2O_2 through the catalysis of myeloperoxidase.[30] Therefore, they have the similar evolution trends at the temporal and dose scales.

Meanwhile, Figure 5B and D also show that the fluorescence intensity from the cyan channel is stronger than that from the green channel. In appearance, the emission intensity of green looks like higher than that of cyan (Figure S18), but the cyan collection window of 60 nm (430−490 nm) is broader than the green one of 50 nm (510−560 nm). Also, the quantum yield of cyan (0.42) is slightly higher than that of green (0.34), as listed in Table S1. On the other hand, PMA may stimulate cells to produce more •OH than HClO because the HClO results from the transformation of H_2O_2 through the catalysis of myeloperoxidase.

Profiling •OH and HClO in the Organs of Living Zebrafish. In the process of normal metabolisms, the organs of living organisms can spontaneously produce various ROS. Most of the currently reported researches only demonstrated the possibility of fluorescent imaging by beforehand feeding/injecting ROS or ROS-induced drugs into the organisms. However, the visualization of spontaneous ROS in a normal organism by a fluorescent probe has still to face with the problems of sensitivity and stability of probe as well as its ability of passing through various biological barriers.

Numerous biological reactions occur at the intestine and liver of living animals, resulting in the spontaneous generations of ROS there.[31−33] Here, we tried to simultaneously observe the distributions of spontaneous •OH and HClO in a living zebrafish without any stimulation of drugs. The wild type seven-day old zebrafish were incubated in aqueous FHZ, and then washed and cultured in water. At the initial stage, the zebrafish were almost nonfluorescent from both cyan and green channels (Figure 6A). At 6 h, the fluorescences from cyan and green channels in intestine reached the highest intensity, while the fluorescences remained relatively weak in liver and pronephros. At 12 h, the fluorescences in intestine gradually decreased in comparison with those at 6 h, but the fluorescences in liver and pronephros became much stronger and the highest intensity reached in liver. After 18 h, the fluorescences from cyan and green channels in intestine and liver continuously decreased, while the fluorescences in pronephros obviously increased to its maximum. Finally, the fluorescences from cyan and green channels in the three organs almost disappeared after about 24 h. These detailed observations suggest that the probe can be first located in intestine and also absorbed into blood, and then transferred/located in liver, and finally the reacted probe was excreted outside zebrafish through pronephros. The evolutions of fluorescence intensities in the intestine, liver and pronephros were illustrated in Figure 6, B and C. Just so, the probe can give

DOI: 10.1021/jacs.5b12848
J. Am. Chem. Soc. 2016, 138, 3769−3778

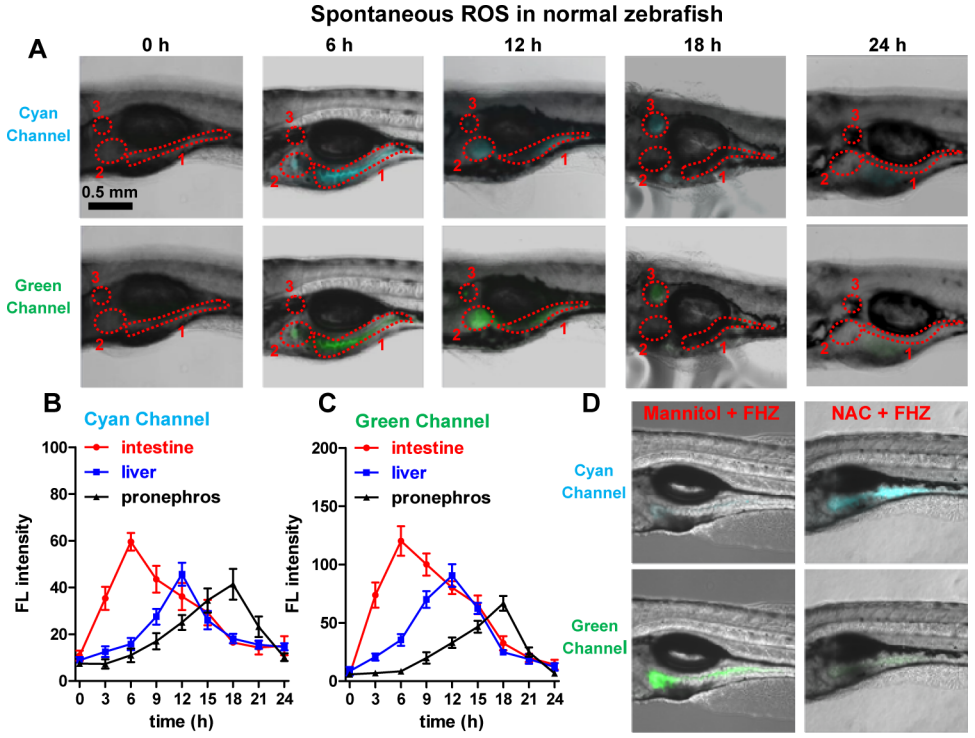

Figure 6. Visualizations of spontaneous ROS in normal zebrafish embryos. The seven-day old zebrafish after fertilization were cultured with 50 μM FHZ in water for 30 min at 28 °C, and then transferred into oxygen-dissolving water (regions: 1, intestine; 2, liver; 3, pronephros). (A) Temporal fluorescent images of FHZ-loaded zebrafish (cyan channel for •OH; green channel for HClO). (B, C) Time-dependent mean fluorescence intensities from cyan and green channels in different organs of zebrafish. The fluorescence intensities were the integrals of fluorescence collected from the whole organs. The mean intensity was obtained from six zebrafish and the error bars represent standard deviation (±SD). (D) The control experiments by the addition of ROS scavengers. Left column: the zebrafish were cultured with 10 mM mannitol (a scavenger of •OH) for 30 min, and then raised in 50 μM FHZ for 30 min. Right column: the zebrafish were cultured with 1 mM NAC (a scavenger of HClO and •OH) for 30 min, and then raised in 50 μM FHZ for 30 min. The photographs were taken after the zebrafish were further cultured for 6 h in water.

the clear profilings of spontaneous •OH and HClO on its transfer pathway.

It should be noted that the bright fluorescences do not certainly indicate the greatest generation of ROS in the intestine and liver, but rather the probes appear to be accumulated and then activated in these regions. Here, three non-ROS-responsive fluorescent probes, fluorescein and its two derivatives (compound 1: fluorescein methyl ester in Scheme 1A; compound 2: triethylene glycol substituted fluorescein methyl ester in Scheme 1A) were selected to see where the probes themselves localized. It was found that the three probes could accumulate in intestine and liver, and further the compound 2 with highly biocompatible lateral chain also accumulated in pronephric region (Figure S26).

In theory, the fluorescences might also be turned on by other biological transformation of probe in the presences of enzymes in living organs. We mixed probe FHZ into the fresh lysates of zebrafish and the mixture was incubated at 28 °C for 4 h, but there was not any fluorescent enhancement observed from the two channels (Figure S27). That is to say, the probe can keep its stability in biological environments and only selectively react with •OH and HClO species. Furthermore, ROS scavengers were also fed to the living zebrafish as the control experiments and the results were shown in Figure 6D. After the living zebrafish were raised in aqueous mannitol (a scavenger of •OH), the fluorescence from cyan channel almost disappeared, but the fluorescence from green channel remained still very strong. After living zebrafish were raised in aqueous NAC, the cyan fluorescence was still relatively strong, while the green fluorescence was very weak, not completely disappeared. Here, the concentration of NAC used was 1 mM, because the higher amount of NAC would cause the death of zebrafish. However, the level of ROS in living zebrafish is much higher than that in cells, and thus the amount of NAC in zebrafish is obviously insufficient for completely scavenging ROS. Moreover, a living zebrafish has much higher capability to continuously produce ROS than single cells. On the other hand, •OH has an extremely short lifetime and thus it cannot accumulate in a living zebrafish. On the contrary, HClO has a much longer lifetime and thus can accumulate in a living zebrafish. That is to say, after the reaction with NAC, the accumulated HClO in zebrafish is mostly consumed. With the subsequent addition of FHZ, the green fluorescence from the reaction of probe with HClO becomes much weaker relative to that in Figure 6A. However, the cyan fluorescence remains similar in fluorescence intensity to that in Figure 6A, because the two cyan fluorescences identically only result from the timely produced •OH after the addition of the probe. The organ-specific and time-dependent analysis on the control experiments are shown in Figure S28.

Visualization of •OH at Fresh Wound of Zebrafish. It is well-known that environmental stress such as external injuries can drive a living organism to release a large amount of ROS in a short time to combat infection and repair damaged tissues.[2,34] However, to directly visualize the release of ROS at injury has been very difficult by a fluorescent probe, because most of ROS are of short lifetimes, e.g., the •OH at time scale of several nano seconds. In the present experiment, living zebrafish were raised

DOI: 10.1021/jacs.5b12848
J. Am. Chem. Soc. 2016, 138, 3769−3778

in aqueous FHZ for 30 min, by which probe FHZ entered the whole tissues of zebrafish, and then a fresh wound was cut at its ventral fin using a thin blade. The wound of fin emitted strong fluorescence from cyan channel, while there was no fluorescence detected from green channel (Figure 7A–C).

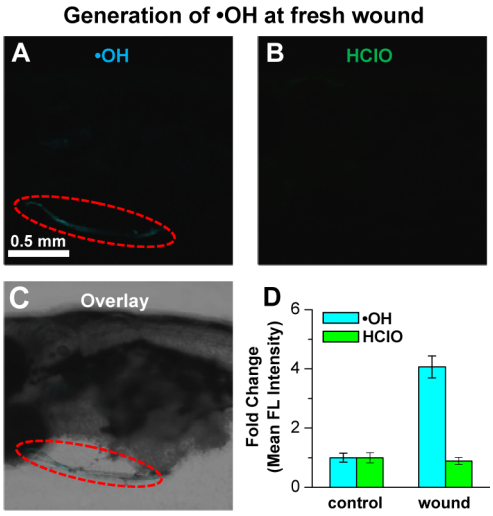

Figure 7. Visualization of •OH released from the fresh wound of zebrafish. Living zebrafish were cultured in 50 μM aqueous FHZ for 30 min, and then a small wound was cut at its ventral fin using a blade. (A) Fluorescent image of wound region from cyan channel. (B) Fluorescent image of wound region from green channel. (C) Overlay of bright-field and cyan-channel images. (D) The mean fluorescence intensity suggesting the generation of •OH at the wound by the comparison with that obtained by control zebrafish. The fluorescence intensities of whole wound were collected, and six parallel experiments were carried out. The error bars represent standard deviation (±SD).

The wound of control zebrafish did not display any fluorescent signals from the cyan and green channels. Together with the data of fluorescence intensities (Figure 7D), these confirm that the fresh wound released a large amount of •OH rather than HClO. To the best of our knowledge, it is the first time to visualize the release of •OH at the wound of zebrafish by fluorescent imaging. Once again, the results provide a conclusive evidence that the probe FHZ can rapidly be absorbed into the blood circulation system from the zebrafish intestine, and spread out whole zebrafish tissues, and keep its stability in the blood, organs and tissues in the absence of ROS.

Discussion on the Difficulties and Weaknesses of This Study. In control experiments, although we have mannitol, a selective scavenger to •OH in the coexistence of •OH and HClO, a scavenger specific to HClO in a system with the coexistence of •OH and HClO has not yet been found from the reported literatures and by our experimental attempts, because •OH has a much stronger oxidativity than that of HClO. The change of the addition order of •OH and HClO in the presence of scavenger NAC provides an indirect evidence to show that the green fluorescence signal comes from the presence of HClO. On the other hand, we agree that the interactions of probes/NAC with a living system are very complicated with potential to produce the proteins or other species with weak fluorescence, which is not completely excluded and thus causes the imperfect selectivity in the fluorescent imaging of •OH and HClO. That is to say, we can not give a full confirmation that the fluorescence signals thoroughly exclude the nonselective reactions of probe in living systems. Therefore, highly specific scavengers in the control experiments should be searched continuously in future.

CONCLUSIONS

In summary, we have synthesized a novel fluorescent probe by reconstructing and modifying a common dye molecule, and developed its fluorescent imaging applications in the real-time discrimination and versatile profiling of multiple ROS in living systems. The probe with dual reactive sites can simultaneously react with two ROS and display different fluorescent responses, which exhibits three remarkable features: (1) the distinguishable ability in the coexistence of two ROS; (2) the rapid, sensitive and dynamic responses; (3) the high biocompatibility of passing through various biological barriers into cells/mitochondria, blood, organs and tissues. On the basis of advantages, the dual-channel imaging provides the real-time observations to the synchronous generations of ROS in cellular mitochondria and the quantitative investigations to clarify their relationship. Along the transfer way of probe, the distributions of spontaneous ROS in the organs of a normal-state zebrafish are clearly revealed by the accumulation of probes there. Moreover, it has been demonstrated for the first time that the release of •OH from the fresh wound of a living zebrafish is visualized in spite of its extremely short lifetime. These successful/unique applications prospect that the versatile probe will be a powerful tool in the investigations of ROS in living systems.

EXPERIMENTAL SECTION

Synthesis of FHZ. Scheme 1A illustrates the three-step reactions to transform fluorescein molecule into compound 1 to compound 2 and to final FHZ. The details of synthesis and characterization are as follows.

Compound 1. Fluorescein (3.32 g, 0.01 mol) was first dissolved in 100 mL of methanol and concentrated sulfuric acid (1 mL) was added dropwise to the solution and refluxed for 12 h. Then the solution was poured into 500 mL water and the mixture was adjusted to pH ~ 7 by $NaHCO_3$. The resulting precipitate was purified through a silica gel column eluted with CH_2Cl_2/CH_3OH (V:V = 8:1). IR (KBr, cm^{-1}): 3452, 1707, 1640, 1606, 1461, 1388, 1319, 1287, 1170, 1138, 759, 668. ^1H NMR (400 MHz, DMSO-d_6, δ): 8.315–8.296 (d, J = 7.6 Hz, 1H, −ArH), 7.976–7.940 (t, 1H, −ArH), 7.903–9.866 (t, 1H, −ArH), 7.567–7.548 (d, J = 7.6 Hz, 1H, −ArH), 7.276–7.253 (d, J = 9.2 Hz, 2H, −ArH), 7.186 (s, 2H, −ArH), 7.064–7.042 (d, J = 8.8 Hz, 2H, −ArH), 3.578 (s, 3H, $-OCH_3$). HR-MS (m/z, ESI) Calculated for $C_{21}H_{13}O_5$ m/z = 347.0919 [M + H]. Found m/z = 347.0914.

Compound 2. 2-[2-(2-Chloroethoxy)ethoxy]ethanol (0.34 g, 2.0 mmol), K_2CO_3 (0.27 g, 2.0 mmol) and compound 1 (0.35 g, 1.0 mmol) were added into 15 mL DMF and stirred at 120 °C for 12 h. Then the solvent was removed under reduced pressure and the product was purified through a silica gel column eluted with AcOEt/CH_3OH (V:V = 20:1). IR (KBr, cm^{-1}): 3430, 2919, 1725, 1642, 1591, 1504, 1479, 1401, 1260, 1110, 1081, 853, 662, 616, 571. ^1H NMR (400 MHz, DMSO-d_6, δ): 8.243 (s, 1H, −ArH), 7.893–7.820 (d, J = 29.2 Hz, 2H, −ArH), 7.530 (s, 1H, −ArH), 7.256 (s, 1H, −ArH), 6.918–6.258 (m, 5H, −ArH), 4.605–4.086 (t, 2H, $-ArOCH_2-$), 3.801 (s, 3H, $-OCH_3$), 3.600–3.369 (m, 10H, $-OCH_2-$). HR-MS (m/z, ESI) Calculated for $C_{27}H_{27}O_8$ m/z = 477.4985 [M − H]. Found m/z = 477.4990.

Probe FHZ. Compound 2 (0.24 g, 0.50 mmol) was dissolved in 8 mL methanol, followed by the addition of 0.5 mL hydrazine hydrate, and stirred at room temperature for 4 h. The solvent was removed under reduced pressure and the product was washed three times with water. The pink solid was obtained in 82% yield. IR (KBr, cm^{-1}): 3415, 2926, 1701, 1637, 1618, 1400, 1184, 1106, 621. ^1H NMR (400 MHz, $CDCl_3$, δ): 7.954 (s, 1H, −ArH), 7.487 (d, 2H, −ArH), 7.056

DOI: 10.1021/jacs.5b12848
J. Am. Chem. Soc. 2016, 138, 3769–3778

(s, 1H, −ArH), 6.711 (s, 2H, −ArH), 6.561−6.488 (m, 4H, −ArH), 4.126 (s, 2H, $-NH_2$), 3.870−3.640 (m, 12H, $-OCH_2-$). ^{13}C NMR (400 MHz, DMSO-d_6, δ): 165.985, 159.618, 158.786, 152.952, 152.825, 133.146, 129.821, 128.988, 128.458, 123.909, 122.892, 112.663, 112.080, 110.282, 102.839, 101.878, 72.843, 70.419, 70.255, 69.290, 67.982, 65.045, 60.689. HR-MS (m/z, ESI) Calculated for $C_{27}H_{25}O_8$ m/z = 477.1662 [M − H]. Found m/z = 477.1556.

Preparation of Intermediate Product FHZ−OH. FHZ (47.8 mg, 0.1 mmol) and $FeSO_4 \bullet 7H_2O$ (54.0 mg, 0.2 mmol) were dissolved in 10 mL water saturated with N_2 atmosphere. Then, 20 μL of H_2O_2 (30%) was injected into the mixture. After stirred at the iced bath for 1 min, the solvent was removed under reduced pressure and the product was purified through a silica gel column eluted with AcOEt. ^1H NMR (400 MHz, DMSO-d_6, δ): 8.027−8.008 (d, 1H, −ArH), 7.807−7.733 (m, 2H, −ArH), 7.293−7.274 (d, 1H, −ArH), 6.959 (s, 1H, −ArH), 6.717−6.588 (m, 4H, −ArH), 4.171 (s, 2H, −OH), 3.762 (s, 2H, $-NH_2$), 3.596−3.428 (m, 12H, $-OCH_2-$). MS (m/z, ESI) Calculated for $C_{26}H_{27}N_2O_8$ m/z = 495.18 [M + H]. Found m/z = 495.18.

Cell Cultures. HeLa cells and RAW264.7 macrophages were cultured in high glucose Dulbecco's modified Eagle's medium (DMEM, Invitrogen, Carlsbad, CA) supplied with 10% fetal bovine serum (FBS, Invitrogen) and 1% antibotics (penicillin and streptomycin) at 37 °C in humidified incubator containing 5% CO_2. The cells were seeded into glass-bottomed dishes and cultured for 24 h. Subsequently, the cells were incubated with FHZ for 30 min at 37 °C and then washed with PBS buffer three times. Each treatment of cells with H_2O_2, EDTA-Fe^{2+}, HClO or scavengers kept 30 min. More experimental details were shown in the results and discussion.

Zebrafish Cultures. Wild type zebrafish was purchased from Wuhan Yisai Biotech. Co., Ltd. Seven-day old fertilized zebrafish embryos were cultured in 50 μM FHZ for 30 min, and then the zebrafish were transferred to fresh water. A FHZ-loaded zebrafish was fixed under confocal microscope using 2% agarose gel to keep its living state for fluorescent imaging. In order to observe the release of •OH in fresh wound, the ventral fin of the FHZ-loaded zebrafish was carefully cut a small wound using a blade. After raised for 20 min in water, the wound of injured zebrafish was imaged using confocal microscope.

■ ASSOCIATED CONTENT

Supporting Information

The Supporting Information is available free of charge on the ACS Publications website at DOI: 10.1021/jacs.5b12848.

Regents and instruments, quantum yields, structural characterizations, spectral analysis, cellular imaging, and zebrafish imaging. (PDF)

■ AUTHOR INFORMATION

Corresponding Author

*zpzhang@iim.ac.cn

Author Contributions

#R.Z., J.Z., and G.H. contributed equally to this work.

Notes

The authors declare no competing financial interest.

■ ACKNOWLEDGMENTS

This work was supported by National Basic Research Program of China (2015CB932002), China-Singapore Joint Project (2015DFG92510), National Natural Science Foundation of China (21335006, 21475135, 21375131, 21275145, 21371174) and Natural Science Foundation of Anhui Province (1408085MKL52, 1508085SQB200, 1608085QB32).

■ REFERENCES

(1) (a) Schiller, H. J.; Reilly, P. M.; Bulkley, G. B. *Crit. Care Med.* **1993**, *21*, S92−S102. (b) Childs, E. W.; Udobi, K. F.; Wood, J. G.; Hunter, F. A.; Smalley, D. M.; Cheung, L. Y. *Shock* **2002**, *18*, 423−427.

(2) McCord, J. M. *Science* **1974**, *185*, 529−531.

(3) (a) Suzuki, Y. J.; Forman, H. J.; Sevanian, A. *Free Radical Biol. Med.* **1997**, *22*, 269−285. (b) Harman, D. *Proc. Natl. Acad. Sci. U. S. A.* **1981**, *78*, 7124−7128.

(4) (a) Floyd, R. A. *Science* **1991**, *254*, 1597−1598. (b) Yoo, S. K.; Starnes, T. W.; Deng, Q.; Huttenlocher, A. *Nature* **2011**, *408*, 109−112.

(5) Dröge, W. *Physiol. Rev.* **2002**, *82*, 47−95.

(6) (a) Valko, M.; Rhodes, C. J.; Moncol, J.; Izakovic, M.; Mazur, M. *Chem.-Biol. Interact.* **2006**, *160*, 1−40. (b) Martindale, J. L.; Holbrook, N. J. *J. Cell. Physiol.* **2002**, *192*, 1−15. (c) Madamanchi, N. R.; Vendrov, A.; Runge, M. S. *Arterioscler., Thromb., Vasc. Biol.* **2005**, *25*, 29−38.

(7) (a) Karasu, C. *Free Radical Biol. Med.* **1999**, *27*, 16−27. (b) Finkel, T.; Serrano, M.; Blasco, M. A. *Nature* **2007**, *448*, 767−774. (c) Halliwell, B.; Gutteridge, J. M. C. *Free Radicals in Biology and Medicine*, 2nd ed.; Oxford University Press: New York, 1989.

(8) Zhang, W.; Li, P.; Yang, F.; Hu, X.; Sun, C.; Zhang, W.; Chen, D.; Tang, B. *J. Am. Chem. Soc.* **2013**, *135*, 14956−14959.

(9) Xu, K.; Qiang, M.; Gao, W.; Su, R.; Li, N.; Gao, Y.; Xie, Y.; Kong, F.; Tang, B. *Chem. Sci.* **2013**, *4*, 1079−1086.

(10) (a) Koide, Y.; Urano, Y.; Hanaoka, K.; Terai, T.; Nagano, T. *J. Am. Chem. Soc.* **2011**, *133*, 5680−5682. (b) Abo, M.; Urano, Y.; Hanaoka, K.; Terai, T.; Komatsu, T.; Nagano, T. *J. Am. Chem. Soc.* **2011**, *133*, 10629−10637.

(11) (a) Yuan, L.; Lin, W.; Xie, Y.; Chen, B.; Zhu, S. *J. Am. Chem. Soc.* **2012**, *134*, 1305−1315. (b) Zhang, Q.; Zhu, Z.; Zheng, Y.; Cheng, J.; Zhang, N.; Long, Y. T.; Zheng, J.; Qian, X.; Yang, Y. *J. Am. Chem. Soc.* **2012**, *134*, 18479−18482.

(12) Sun, M.; Yu, H.; Zhu, H.; Ma, F.; Zhang, S.; Huang, D.; Wang, S. *Anal. Chem.* **2014**, *86*, 671−677.

(13) (a) Srikun, D.; Miller, E. W.; Domaille, D. W.; Chang, C. J. *J. Am. Chem. Soc.* **2008**, *130*, 4596−4597. (b) Albers, A. E.; Okreglak, V. S.; Chang, C. J. *J. Am. Chem. Soc.* **2006**, *128*, 9640−9641.

(14) Pu, K.; Shuhendler, A. J.; Rao, J. *Angew. Chem., Int. Ed.* **2013**, *52*, 10325−10329.

(15) Jiang, C.; Liu, R.; Han, G.; Zhang, Z. *Chem. Commun.* **2013**, *49*, 6647−6649.

(16) Lee, D.; Khaja, S.; Velasquez-Castano, J. C.; Dasari, M.; Sun, C.; Petros, J.; Taylor, W. R.; Murthy, N. *Nat. Mater.* **2007**, *6*, 765−769.

(17) Soh, N.; Makihara, K.; Sakoda, E.; Imato, T. *Chem. Commun.* **2004**, *40*, 496−497.

(18) Tang, B.; Zhang, N.; Chen, Z.; Xu, K.; Zhuo, L.; An, L.; Yang, G. *Chem. - Eur. J.* **2008**, *14*, 522−528.

(19) Zhang, W. J.; Guo, C.; Liu, L. H.; Qin, J. G.; Yang, C. L. *Org. Biomol. Chem.* **2011**, *9*, 5560−5563.

(20) Sun, Z. N.; Liu, F. Q.; Chen, Y.; Tam, P. K. H.; Yang, D. *Org. Lett.* **2008**, *10*, 2171−2174.

(21) (a) Umezawa, N.; Tanaka, K.; Urano, Y.; Kikuchi, K.; Higuchi, T.; Nagano, T. *Angew. Chem., Int. Ed.* **1999**, *38*, 2899−2901. (b) Tanaka, K.; Miura, T.; Umezawa, N.; Urano, Y.; Kikuchi, K.; Higuchi, T.; Nagano, T. *J. Am. Chem. Soc.* **2001**, *123*, 2530−2536.

(22) (a) Zhang, G. X.; Li, X. H.; Ma, H. M.; Zhang, D. Q.; Li, J.; Zhu, D. B. *Chem. Commun.* **2004**, *40*, 2072−2073. (b) Li, X. H.; Zhang, G. X.; Ma, H. M.; Zhang, D. Q.; Li, J.; Zhu, D. B. *J. Am. Chem. Soc.* **2004**, *126*, 11543−11548.

(23) Cossarizza, A.; Ferraresi, R.; Troiano, L.; Roat, E.; Gibellini, L.; Bertoncelli, L.; Nasi, M.; Pinti, M. *Nat. Protoc.* **2009**, *4*, 1790−1797.

(24) Komatsu, H.; Miki, T.; Citterio, D.; Kubota, T.; Shindo, Y.; Kitamura, Y.; Oka, K.; Suzuki, K. *J. Am. Chem. Soc.* **2005**, *127*, 10798−10799.

(25) Ou, B.; Hampsch-Woodill, M.; Prior, R. L. *J. Agric. Food Chem.* **2001**, *49*, 4619−4626.

(26) Eftekhari-Sis, B.; Zirak, M.; Akbari, A. *Chem. Rev.* **2013**, *113*, 2958−3043.

DOI: 10.1021/jacs.5b12848
J. Am. Chem. Soc. 2016, 138, 3769−3778

(27) Zhang, Z.; Zheng, Y.; Hang, W.; Yan, X.; Zhao, Y. *Talanta* **2011**, *85*, 779−786.
(28) Aruoma, O. I.; Halliwell, B.; Hoey, B. M.; Butler, J. *Free Radical Biol. Med.* **1989**, *6*, 593−597.
(29) Yuan, L.; Lin, W.; Song, J. *Chem. Commun.* **2010**, *46*, 7930−7932.
(30) (a) Prokopowicz, Z. M.; Arce, F.; Biedroń, R.; Chiang, C. L.; Ciszek, M.; Katz, D. R.; Nowakowska, M.; Zapotoczny, S.; Marcinkiewicz, J.; Chain, B. M. *J. Immunol.* **2010**, *184*, 824−835. (b) Pattison, D. I.; Davies, M. J. *Biochemistry* **2006**, *45*, 8152−8162.
(31) Palileo, C.; Kaunitz, J. D. *Curr. Opin. Gastroenterol.* **2011**, *27*, 543−548.
(32) Jones, R. M.; Mercante, J. W.; Neish, A. S. *Curr. Med. Chem.* **2012**, *19*, 1519−1529.
(33) Zhu, H.; Li, Y. R. *Exp. Biol. Med.* **2012**, *237*, 474−480.
(34) Niethammer, P.; Grabher, C.; Look, A. T.; Mitchison, T. J. *Nature* **2009**, *459*, 996−999.

DOI: 10.1021/jacs.5b12848
J. Am. Chem. Soc. 2016, 138, 3769−3778